


ARTICLE

<https://doi.org/10.1038/s42005-019-0263-0>

OPEN

Tunable super- and subradiant boundary states in one-dimensional atomic arrays

Anwei Zhang¹, LuoJia Wang¹, Xianfeng Chen^{1,2}, Vladislav V. Yakovlev³ & Luqi Yuan ^{1*}

Efficient manipulation of quantum states is a key step towards applications in quantum information, quantum metrology, and nonlinear optics. Recently, atomic arrays have been shown to be a promising system for exploring topological quantum optics and robust control of quantum states, where the inherent nonlinearity is included through long-range hoppings. Here we show that a one-dimensional atomic array in a periodic magnetic field exhibits characteristic properties associated with an effective two-dimensional Hofstadter-butterfly-like model. Our work points out super- and sub-radiant topological edge states localized at the boundaries of the atomic array despite featuring long-range interactions, and opens an avenue of exploring an interacting quantum optical platform with synthetic dimensions.

¹State Key Laboratory of Advanced Optical Communication Systems and Networks, School of Physics and Astronomy, Shanghai Jiao Tong University, Shanghai 200240, China. ²Collaborative Innovation Center of Light Manipulations and Applications, Shandong Normal University, Jinan 250358, China. ³Texas A&M University, College Station, TX 77843, USA. *email: yuanluqi@sjtu.edu.cn

Atomic arrays refer to an ensemble of atoms where the interaction of atoms and photons takes place¹. The light-atom coupling in atomic arrays exhibits fundamental physical phenomena, including facilitating the long-range coherent interactions and promoting the collective radiative loss². Recent advances in assembling highly ordered one-dimensional (1D) and two-dimensional (2D) atomic arrays provide unique platforms for exploring the light-matter interaction in quantum optics^{3–5}. The interference in the emitted optical field leads to remarkable optical properties such as the subradiant state^{6–9}, a high reflection of radiation^{10–12}, the efficient storage and retrieval for quantum memory¹³, and topologically-protected edge states^{14,15}, which show important applications toward quantum information processing, quantum metrology, and nonlinear optics^{16,17}.

Topological physics is of fundamental importance where physical characteristics are robust against microscopic variation of system details^{18–20}. Related phenomena can be explored by engineering the Hamiltonian of an atomic or optical system^{21–23}. Such approach shows a great potential toward quantum simulation of topological matter. In particular, atomic or optical systems provide a novel fundamental way of manipulating quantum states of the light, such as robust photon transport in photonic systems^{24–27} and non-reciprocal transport in hot atomic gas^{28,29}. Recently, it has been shown that atomic arrays hold a promise for studying topological quantum optics, where the inherent non-linearity brings a natural way to explore the physics including long-range hoppings^{14,15,30–32}.

Robust single-photon super- and subradiant states hold a significant promise for applications related to quantum storage and quantum information. In this paper, we investigate 1D atomic arrays subjected to a spatially periodic magnetic field. The spatial phase of the magnetic field is an external parameter, and can be used to map one momentum dimension in a 2D topological system^{33,34}. Therefore, 1D atomic arrays with the synthetic momentum dimension manifests important optical features associated with 2D systems. Systems with synthetic dimensions simplify experimental design and enable capabilities of manipulating atomic quantum states or photons along the synthetic dimension^{33–38}. By changing the periodicity of the magnetic field, we show that the 1D atomic arrays exhibit a butterfly-like spectrum, which has not been discussed in the 2D atomic arrays under a uniform magnetic field^{14,30}. Such spectrum, associated with the open quantum optical system involving long-range hoppings along the synthetic dimension, exhibits features which are dramatically distinct from the spectrum in the 1D photonic model^{39–41}. For a finite 1D atomic array, the system supports pairs of topological boundary states with opposite circular polarizations, exhibiting super- or subradiance dependent on the magnetic field distribution and atomic excitation frequency, which is found to be persevering with the small disorder involved in simulations. The subradiant state localized at the boundary of atomic arrays provides a potential application toward robust quantum storage against small perturbations. The results discussed here show a route toward the possibility of exploring long-range interacting topological physics in quantum optical system with synthetic dimension.

Results

Formalism. We propose the experimental arrangement consisting of a 1D array of N atoms which are aligned along the y direction with the spacing a . Each atom (labeled by n and located at y_n) has a V-type internal level structure with the ground state $|g_n\rangle$ and excited states $|\pm_n\rangle = \mp(|x_n\rangle \pm i|y_n\rangle)/\sqrt{2}$, where the transition between $|g_n\rangle$ and $|\pm_n\rangle$ is coupled with the right (left)

circularly polarized light. Here $|x(y)\rangle$ refers to the state polarized along the $x(y)$ direction. The degeneracy of the excited states is broken by the presence of an external magnetic field $B_n \equiv B(y_n)$ along the z axis (see Fig. 1a).

We consider the dynamics of single-excited atoms coupled to free-space modes of the radiation field. After integrating out radiation modes under the dipole approximation, one obtains the non-Hermitian effective Hamiltonian^{12,14,30}

$$H = \sum_n \sum_{\alpha=\pm} \left(\omega_0 - i\frac{\gamma_0}{2} + \text{sgn}(\alpha)\mu B_n \right) |\alpha_n\rangle \langle \alpha_n| + \frac{3\pi\gamma_0}{k_0} \sum_{n \neq m} \sum_{\alpha, \beta=\pm} G_{\alpha\beta}(y_n - y_m) |\alpha_n\rangle \langle \beta_m|, \quad (1)$$

where $\omega_0 = k_0 c = 2\pi c/\lambda$ is the atomic transition frequency with the wave vector k_0 and the wavelength λ , γ_0 is the atomic decay rate in the free space, $\text{sgn}(\pm) \equiv \pm$, and μB_n gives the Zeeman shift for the n th atom with the magnetic moment μ . $G_{\alpha\beta}(y_n - y_m)$ is the free-space dyadic Green's function describing the electric field at y_n emitted by the atom located at y_m . By using the Green's

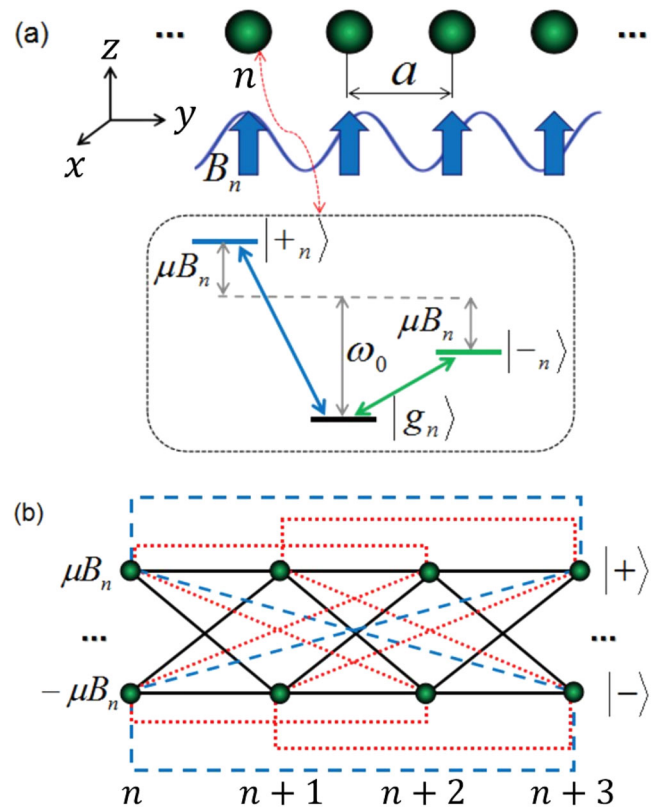


Fig. 1 Schematic of a 1D atomic array in a periodic magnetic field. **a** The atomic array subjected to the external magnetic field B_n , where each atom has a V-type atomic level structure with non-degeneracy excited states $|\pm_n\rangle$ split by the magnetic field. **b** The equivalent tight-binding lattice model with on-site potentials $\pm B_n$ and photon-mediated long-range hoppings. Black solid, red dotted and blue dashed lines label the nearest-neighbor, next-nearest-neighbor and triatomic spacing hoppings, respectively, indicating dipole-dipole interactions and collective dissipations.

function in Cartesian basis^{7,30,31,42}, one has

$$G_{\pm\pm} = \frac{G_{xx} + G_{yy}}{2} = -\frac{e^{ik_0 r}}{8\pi k_0^2 r^3} (k_0^2 r^2 - ik_0 r + 1),$$

$$G_{\pm\mp} = \frac{G_{yy} - G_{xx}}{2} = \frac{e^{ik_0 r}}{8\pi k_0^2 r^3} (k_0^2 r^2 + 3ik_0 r - 3),$$
(2)

where $r = |y_n - y_m|$.

The atomic system under investigation is an effective tight-binding lattice model (see Fig. 1b). The photon-mediated long-range hoppings amplitude is described by coefficients in the last term of the Hamiltonian, where the real part describes photon-mediated dipole-dipole interaction potential between the n th and m th atoms, while the imaginary part denotes the collective dissipative rate of the two atoms.

To construct the spectrum of the non-Hermitian Hamiltonian in Eq. (1), we take the linear combination of single-excited states $|\psi\rangle = \sum_n (C_{n,+}|+n\rangle + C_{n,-}|-n\rangle)$, where $C_{n,\pm}$ is the amplitude of the wave function for the n th atom with the \pm polarization. The spectrum can be calculated by using the time-independent Schrödinger equation $H|\psi\rangle = E|\psi\rangle$, which leads to

$$EC_{n,+} = \frac{3\pi\gamma_0}{k_0} \sum_{l \neq 0} [G_{++}(la)C_{n+l,+} + G_{+-}(la)C_{n+l,-}]$$

$$+ \left(\omega_0 - i\frac{\gamma_0}{2} + \mu B_n \right) C_{n,+},$$

$$EC_{n,-} = \frac{3\pi\gamma_0}{k_0} \sum_{l \neq 0} [G_{-+}(la)C_{n+l,+} + G_{--}(la)C_{n+l,-}]$$

$$+ \left(\omega_0 - i\frac{\gamma_0}{2} - \mu B_n \right) C_{n,-},$$
(3)

where l is a non-zero integer. $E \equiv \omega - i\gamma/2$ is the complex eigenvalue, in which ω denotes the self-energy of the collective atomic excitation and γ is the collective decay rate of the system.

We consider a spatially periodic magnetic field

$$B_n = B(y_n) = B_0 \cos(2\pi bn + \phi),$$
(4)

where B_0 is the field amplitude, the parameter b controls the periodicity of the magnetic field, and ϕ is the modulation phase. By applying the magnetic field with different spatial shapes along the y direction, one has the control of parameters b and ϕ . Here ϕ provides an additional degree of freedom to our system serving the purpose of the synthetic dimension, so the system can be explored by exploiting the parameter-dependency of the Hamiltonian^{33,34}. In such a synthetic space, b gives the effective magnetic flux while ϕ denotes a synthetic momentum dimension^{40,43}. Hence we can study the physics associated with an open 2D system with long-range couplings under the effective magnetic flux.

Spectra of the non-Hermitian Hamiltonian. We plot the spectrum projected over the synthetic momentum dimension ϕ while varying b in Fig. 2. The parameters are $a = 0.1\lambda$ and $\mu B_0 = 10\gamma_0$ ¹⁴, and spectrum is computed by following the method by Hofstadter⁴⁴ for the atomic array with $N = 150$ under a periodic boundary condition and also choosing b as rational numbers from 0 to 1. Hoppings in Eq. (2) are long-range but decay as $1/r$, we then make truncation in the calculation to get rid of the divergence in the spectrum. One can see the resulting butterfly-like spectrum (ω), which exhibits multiple bulk bands and gaps for each b . As compared with the original Hofstadter-butterfly bandstructure⁴⁴ and also the butterfly-like spectrum in the 1D photonic model³⁹, the spectrum in Fig. 2 shows the open and close of the bandgap with the difference in subtleties while b is varying even with the presence of the long-range non-Hermitian couplings in the atomic arrays.

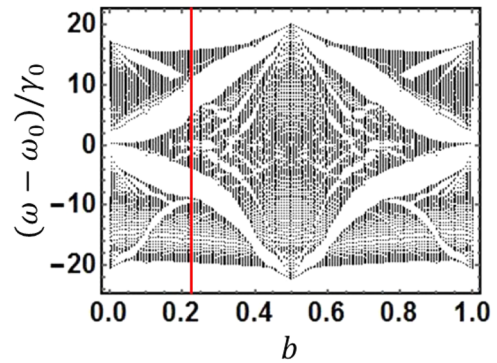


Fig. 2 The numerically calculated spectrum. The spectrum ω is projected over the synthetic momentum dimension ϕ , which is the modulation phase, versus the parameter b in the external magnetic field with the spacing $a = 0.1\lambda$ and the magnetic field amplitude $\mu B_0 = 10\gamma_0$. ω_0 denotes the atomic transition frequency and γ_0 denotes the atomic decay rate in the free space. Red line corresponds to $b = \sqrt{5}/10$.

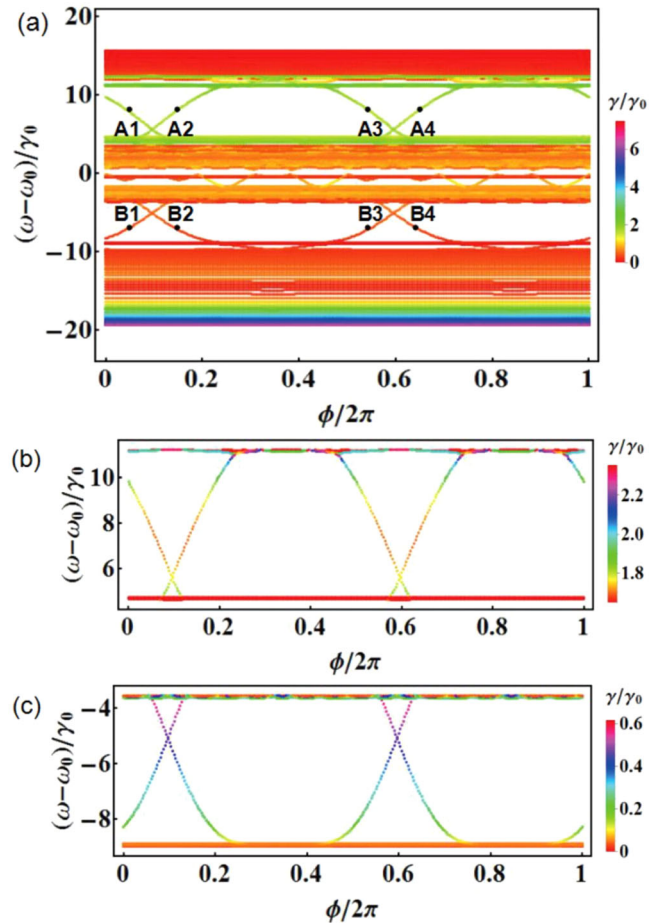


Fig. 3 The spectrum with $b = \sqrt{5}/10$. **a** The spectrum ω as a function of the modulation phase ϕ under open boundary condition for an atomic array with the atomic number $N = 101$ and the spacing $a = 0.1\lambda$. The applied external magnetic field has parameters $\mu B_0 = 10\gamma_0$ and $b = \sqrt{5}/10$. A1, A2, A3, A4 and B1, B2, B3, B4 label a variety of boundary states with $(\omega - \omega_0)/\gamma_0 = 8.15$ and -7.21 , respectively, at different ϕ . **b, c** The zoom-in spectra, showing the details of boundary states. The color of the spectrum gives the collective decay rate γ . ω_0 denotes the atomic transition frequency and γ_0 denotes the atomic decay rate in the free space.

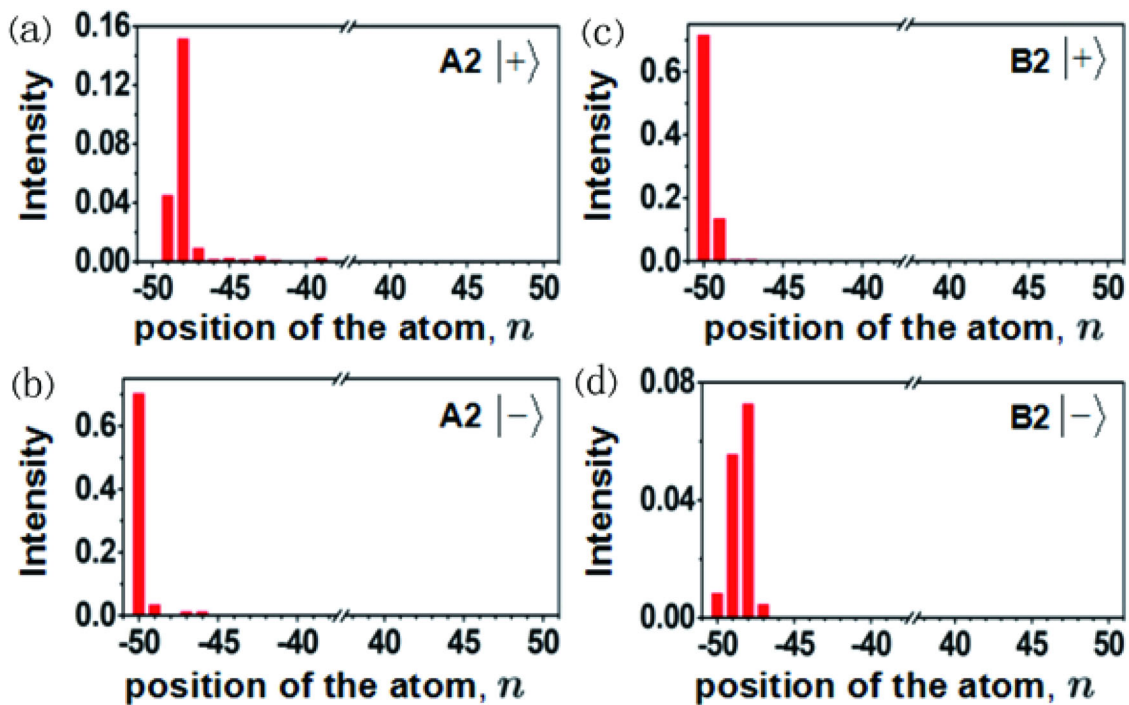


Fig. 4 The study of intensity distributions of boundary states. **a, b, c, d** Intensity distributions of $|+\rangle$ and $|-\rangle$ excited states on the n th atom, which corresponds to the boundary state labeled by A2 (B2), where A2 and B2 denote $[\phi/2\pi, (\omega - \omega_0)/\gamma_0] = (0.15, 8.15)$ and $(0.15, -7.21)$, respectively. Both boundary states are localized on the left boundary of the atomic arrays. ϕ denotes the modulation phase, ω denotes the self-energy of the collective atomic excitation, ω_0 denotes the atomic transition frequency, and γ_0 denotes the atomic decay rate in the free space.

The parameter b can be externally adjusted by controlling the magnetic field. Once it is irrational, the effective magnetic flux is incommensurate with the lattice and the system exhibits a quasicrystal structure⁴⁰. We set $b = \sqrt{5}/10$, indicated by the red line in Fig. 2. In Fig. 3a, the spectrum of the lattice is plotted under an open boundary condition with $N = 101$ against the modulation phase ϕ in the external magnetic field. As a consequence of the presence of the magnetic field which breaks the time-reversal symmetry of the system, one can see that there is a fractal set of band gaps, and, inside each gap, it exhibits pairs of topological boundary states. Moreover, the striking characteristic of this structure is that the collective decay rate (γ) is changing for different ω and ϕ , covering the range from 0 to $\sim 7.5\gamma_0$. The destructive interference in the atom-photon interaction leads to suppressed radiative loss for certain states, corresponding to subradiant states with decay rate below the single-atom emission rate γ_0 . In particular, the collective decay rates γ for boundary states in two larger gaps show different physical features. The boundary states inside the upper gap has $\gamma > \gamma_0$, corresponding to superradiant modes with enhanced collective emission, while the boundary states inside the lower gap are subradiant because γ is smaller than γ_0 . Moreover, the collective decay rate is also changing along each boundary state when one varies the parameter ϕ , as shown in Fig. 3b, c. In particular, for the subradiant boundary states in the lower gap, as indicated in Fig. 3c, γ changes from $\sim 0.6\gamma_0$ to $\sim 0.1\gamma_0$, showing a significant suppression of the spontaneous emission. Furthermore, the lifetimes of boundary states are influenced by the choice of the parameter b . For instance, for the case $b = (\sqrt{3} - 1)/2$, the boundary states inside the two large gaps are both subradiant (see Supplementary Note 1).

The aforementioned boundary states are localized on the left or right boundary of the lattice with a combination of $|+\rangle$ and $|-\rangle$

excited states. As an example, in Fig. 4, we plot the intensity distributions of boundary states from the eigenfunction analysis versus the position of the atom n for $|\pm\rangle$ excited states labeled by A2 and B2 in Fig. 3a, which correspond to superradiant and subradiant states, respectively. The superradiant boundary state A2 is located mainly at the $|-\rangle$ excited state on the leftmost atom, while a small portion of the intensity is distributed at $|+\rangle$ on other atoms near the left boundary due to the hoppings between the two excited states on different atoms. We denote the boundary state A2 by L_- then. Similarly, the subradiant boundary state B2 is located mainly at the $|+\rangle$ excited state on the leftmost boundary, and hence is labeled by L_+ . The two boundary states corresponding to the same ϕ but different excitation frequency, so one can selectively excite either the superradiant or subradiant boundary states for a given external magnetic field.

Other boundary states labeled by A1, A3, A4 in the upper gap and B1, B3, B4 in the lower gap, as shown in Fig. 3a, give R_- (mainly distributed at $|-\rangle$ on the right boundary), R_+ (mainly distributed at $|+\rangle$ on the right boundary), L_+ and R_+ , R_- , L_- , respectively. One therefore can selectively prepare a super- or subradiant state with either right or left circular polarization by a choice of ϕ as well as the excitation frequency of the source field, which we will demonstrate in numerical simulations. In each gap, the boundary states located at the same boundary with opposite polarization excitations exhibit slopes of edge states being both either positive or negative, while the boundary states at different boundaries support edge states having slopes with the opposite sign.

Simulations. We further perform numerical simulations with solving the time-dependent Schrödinger equation $H|\psi(t)\rangle = id|\psi(t)\rangle/dt$, where $|\psi(t)\rangle = \sum_n (C_{n,+}(t)|+\rangle_n + C_{n,-}(t)|-\rangle_n)$ and

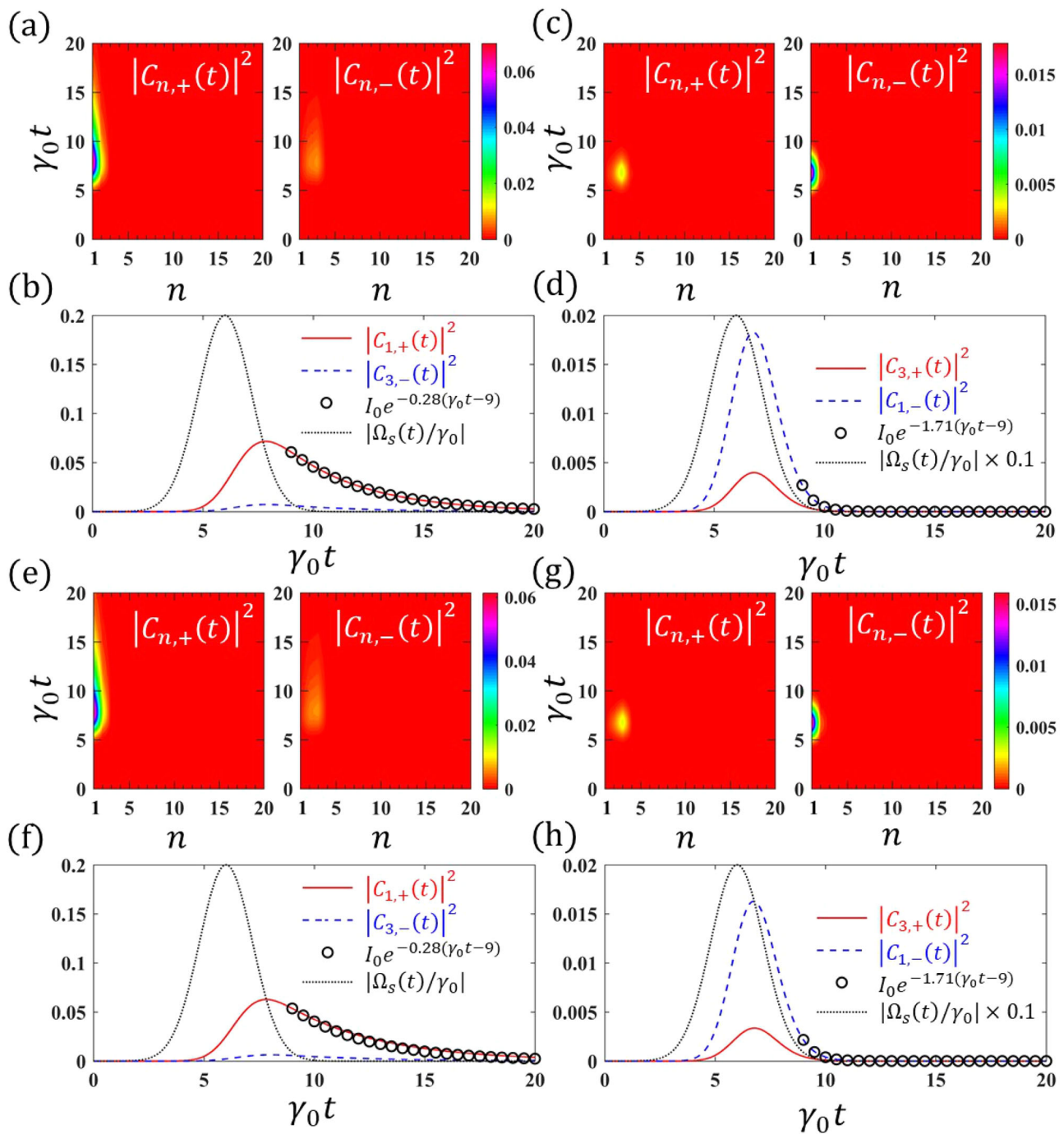


Fig. 5 Simulation results of intensity distributions. **a** Normalized intensity distributions $|C_{n,+}(t)|^2$ and $|C_{n,-}(t)|^2$ on the n th atom versus the time t , where the source field is applied on the leftmost atom, having the frequency detuning $\Delta\omega/\gamma_0 = -7.21$ with the temporal envelope $\Omega_s(t)$ in **b**. γ_0 denotes the atomic decay rate in the free space. **b** Evolutions of $|C_{1,+}(t)|^2$ and $|C_{3,-}(t)|^2$ under a fitting with $I_0 = |C_{1,+}(\gamma_0 t = 9)|^2$, respectively. **c** $|C_{n,+}(t)|^2$ and $|C_{n,-}(t)|^2$ versus t , where the source field has the frequency detuning $\Delta\omega/\gamma_0 = 8.15$. **d** Evolutions of $|C_{1,-}(t)|^2$ and $|C_{3,+}(t)|^2$ under a fitting with $I_0 = |C_{1,-}(\gamma_0 t = 9)|^2$, respectively. **e-h** Simulation results similar to **a-d** but the location of each atom being shifted at a random number within 5% along the y -axis in the atomic array.

H is defined in Eq. (1). The physical system is chosen to be the same as that explored in Fig. 4, where $n = 1, \dots, 101$, $b = \sqrt{5}/10$, and $\phi/2\pi = 0.15$. A gaussian-shape source field $\Omega_s(t)$ is applied to excite both $|\pm\rangle$ states on the leftmost atom with a tunable frequency detuning $\Delta\omega$. The Rabi frequency of the source field is chosen to be small enough so that the excitation of the system follows mainly on the collective decay from the system rather than the Rabi oscillation. In Fig. 5a, we show

the simulated dynamics of intensity distributions $|C_{n,+}(t)|^2$ and $|C_{n,-}(t)|^2$ for n from 1 to 20, with $\Omega_s(t)$ having the temporal envelope in Fig. 5b and $\Delta\omega/\gamma_0 = -7.21$, which aims to excite the subradiant boundary state B2 in Fig. 4. The simulation result shows that the excitation is localized mostly on the intensity $|C_{1,+}|^2$, while a small portion of the intensity is extended to $|C_{3,-}|^2$. $|C_{n,\pm}(t)|^2$ for $n > 20$ is also nearly zero. Furthermore,

Fig. 5b shows evolutions of $|C_{1,+}(t)|^2$ and $|C_{3,-}(t)|^2$. $|C_{1,+}(t)|^2$ is fitted with the decay function $e^{-0.28\gamma_0 t}$ from $\gamma_0 t = 9$, when the source field passes, so the affect from the source excitation is mostly prevented. From the plot, one can see that the tail of $|C_{1,+}(t)|^2$ follows the decay at a collective rate $0.28\gamma_0$. Hence the subradiant boundary state B2 demonstrated in the simulation is consistent with the eigenfunction analysis in Fig. 4. Such selectively prepared subradiant state localized at the boundary of the arrays, is robust against small variations of the system. It therefore shows a potential for the robust quantum storage, which is of great importance for quantum device applications.

We then perform the simulation using $\Omega_s(t)$ with $\Delta\omega/\gamma_0 = 8.15$, and plot results in Figs. 5c, d. $|C_{1,-}|^2$ is mostly excited, which decays at a rate $\sim 1.71\gamma_0 t$ in the fitting. The simulation result shows the superradiant boundary state A2 in Fig. 4. From this set of simulations, we show that, such super- or subradiant boundary state is localized at the boundary of atomic arrays. Moreover, by tuning the frequency detuning $\Delta\omega$ of the source field, one indeed can selectively excite the subradiant state with the right circular polarization or the superradiant state with the left circular polarization.

To show that the proposed system is robust against small disorder, we perform simulations with the same atomic arrays in Figs. 5a–d, but the location of each atom being shifted at a random number within $\delta = 5\%$ along the y -axis. The corresponding simulation results are plotted in Figs. 5e–h, where one can see that the features of subradiant/superradiant boundary state still exhibit.

The excitation of boundary states depends on the choice of $\Delta\omega$. For the same system in Figs. 5a–d, we can also excite the bulk state by choosing $\Delta\omega/\gamma_0 = -10$, where the intensities of the excitation $|C_{n,\pm}(t)|^2$ evolve toward the middle of the atomic array. On the other hand, further increase of disorder can destroy the subradiant/superradiant boundary state. We find that, for disorder with $\delta = 20\%$, the features in the excitation dynamics corresponding to subradiant/superradiant phenomena from couplings between atoms in the entire array no longer persist (see Supplementary Note 2). Moreover, not only pulsed source can excite the desired boundary states, we notice that the continuous-wave (CW) laser can also be used to prepare such boundary states.

Discussion

The proposed system is experimentally feasible. For example, an atomic array with the subwavelength-scale lattice spacing can be realized by using bosonic strontium^{45,46}. The transition between triplet states 3P_0 and 3D_1 of atom ^{84}Sr gives emission at the wavelength $\lambda = 2.6 \mu\text{m}$. One can use the optical lattice formed by lasers at 412.8 nm to trap the atoms, which achieves a sub-wavelength lattice spacing $a = 206.4 \text{ nm}$, i.e., $a/\lambda \approx 0.08$ ⁴⁵. Inhomogeneous magnetic field is widely used to produce spin-orbit couplings in the condensed matter systems^{47,48}. The magnetic field in Eq. (4) can be implemented by a variety of experimental technologies which have been proposed to construct magnetic lattices^{49–53}. One can use either a CW or pulsed laser at a frequency resonant with the boundary state L_{\pm} (R_{\pm}) inside the bandgap to excite the $|\pm\rangle$ state of the atom located at the left (right) boundary. The emission of such super- or subradiant boundary state is localized at the boundary of atomic arrays with the enhanced or suppressed collective decay rate.

In summary, we have investigated 1D atomic arrays subjected to the spatially periodic magnetic field, which supports the non-Hermitian lattice model with long-range hoppings. The phase in the magnetic field serves as an external parameter, which gives a

synthetic momentum dimension. In atomic arrays with long-range hoppings, the existence of topological edge states is not generally valid¹⁵. In the open system proposed here, we consider a synthetic space including one spatial dimension and one synthetic momentum dimension. By carefully selecting parameters, we show that this synthetic space exhibits pairs of topological boundary states, which holds fundamentally different physics from the 1D atomic arrays with a non-zero Zak phase³¹. These boundary states are localized at the boundary of atomic arrays and exhibit super- or subradiance with right or left circular polarization, which can be robust against small disorder in simulations. Our results show potential applications toward manipulating atomic emission at the single-photon level in atomic arrays with the concept of synthetic dimensions, which is important for the quantum memory and quantum information, and also leads potential implications for quantum sensors^{54,55} and super-resolution spectroscopy⁵⁶ by using the robust single-photon superradiant states. The study of quantum optics with synthetic dimensions opens a route of possibly exploring topological phenomena in versatile higher-dimensional strong-interacting open quantum systems in the future.

Data availability

The data that support the findings of this study are available from the corresponding author on request.

Received: 13 July 2019; Accepted: 26 November 2019;

Published online: 12 December 2019

References

- Lamb, Jr. W. E. & Retherford, R. C. Fine structure of the hydrogen atom by a microwave method. *Phys. Rev.* **72**, 241 (1947).
- Dicke, R. Coherence in spontaneous radiation processes. *Phys. Rev.* **93**, 99 (1954).
- Xia, T. et al. Randomized benchmarking of single-qubit gates in a 2D array of neutral-atom qubits. *Phys. Rev. Lett.* **114**, 100503 (2015).
- Endres, M. et al. Atom-by-atom assembly of defect-free one-dimensional cold atom arrays. *Science* **354**, 1024 (2016).
- Barredo, D., de Léséleuc, S., Lienhard, V., Lahaye, T. & Browaeys, A. An atom-by-atom assembler of defect-free arbitrary two-dimensional atomic arrays. *Science* **354**, 1021 (2016).
- Facchinetti, G., Jenkins, S. D. & Ruostekoski, J. Storing light with subradiant correlations in arrays of atom. *Phys. Rev. Lett.* **117**, 243601 (2016).
- Asenjo-García, A., Moreno-Cardoner, M., Albrecht, A., Kimble, H. J. & Chang, D. E. Exponential improvement in photon storage fidelities using subradiance and “selective radiance” in atomic arrays. *Phys. Rev. X* **7**, 031024 (2017).
- Zhang, Y.-X. & Mølmer, K. Theory of subradiant states of a one-dimensional two-level atom chain. *Phys. Rev. Lett.* **122**, 203605 (2019).
- Guimond, P.-O., Grankin, A., Vasilyev, D. V., Vermersch, B. & Zoller, P. Subradiant bell states in distant atomic arrays. *Phys. Rev. Lett.* **122**, 093601 (2019).
- García De Abajo, F. J. Colloquium: light scattering by particle and hole arrays. *Rev. Mod. Phys.* **79**, 1267 (2007).
- Bettles, R. J., Gardiner, S. A. & Adams, C. S. Enhanced optical cross section via collective coupling of atomic dipoles in a 2D array. *Phys. Rev. Lett.* **116**, 103602 (2016).
- Shahmoon, E., Wild, D. S., Lukin, M. D. & Yelin, S. F. Cooperative resonances in light scattering from two-dimensional atomic arrays. *Phys. Rev. Lett.* **118**, 113601 (2017).
- Manzoni, M. T. et al. Optimization of photon storage fidelity in ordered atomic arrays. *N. J. Phys.* **20**, 083048 (2018).
- Perczel, J. et al. Topological quantum optics in two-dimensional atomic arrays. *Phys. Rev. Lett.* **119**, 023603 (2017).
- Bettles, R. J. et al. Topological properties of a dense atomic lattice gas. *Phys. Rev. A* **96**, 041603 (2017). (R).
- Hammerer, K., Sørensen, A. S. & Polzik, E. S. Quantum interface between light and atomic ensembles. *Rev. Mod. Phys.* **82**, 1041 (2010).
- Ohl de Mello, D. et al. Defect-free assembly of 2D clusters of more than 100 single-atom quantum systems. *Phys. Rev. Lett.* **122**, 203601 (2019).

18. Klitzing, K. V., Dorda, G. & Pepper, M. New method for high-accuracy determination of the fine-structure constant based on quantized hall resistance. *Phys. Rev. Lett.* **45**, 494 (1980).
19. Tsui, D. C., Stormer, H. L. & Gossard, A. C. Two-dimensional magnetotransport in the extreme quantum limit. *Phys. Rev. Lett.* **48**, 1559 (1982).
20. Laughlin, R. B. Anomalous quantum hall effect: an incompressible quantum fluid with fractionally charged excitations. *Phys. Rev. Lett.* **50**, 1395 (1983).
21. Ozawa, T. et al. Topological photonics. *Rev. Mod. Phys.* **91**, 015006 (2019).
22. Cooper, N. R., Dalibard, J. & Spielman, I. B. Topological bands for ultracold atoms. *Rev. Mod. Phys.* **91**, 015005 (2019).
23. Zhang, D.-W., Zhu, Y.-Q., Zhao, Y. X., Yan, H. & Zhu, S.-L. Topological quantum matter with cold atoms. *Adv. Phys.* **67**, 253 (2019).
24. Wang, Z., Chong, Y., Joannopoulos, J. D. & Soljačić, M. Observation of unidirectional backscattering-immune topological electromagnetic states. *Nature* **461**, 772 (2009).
25. Hafezi, M., Demler, E., Lukin, M. & Taylor, J. Robust optical delay lines with topological protection. *Nat. Phys.* **7**, 907 (2011).
26. Fang, K., Yu, Z. & Fan, S. Realizing effective magnetic field for photons by controlling the phase of dynamic modulation. *Nat. Photonics* **6**, 782 (2012).
27. Rechtsman, M. C. et al. Photonic Floquet topological insulators. *Nature* **496**, 196 (2013).
28. Wang, D.-W. et al. Topological phase transitions in superradiance lattices. *Optica* **2**, 712 (2015).
29. Cai, H. et al. Experimental observation of momentum-space chiral edge currents in room-temperature atoms. *Phys. Rev. Lett.* **122**, 023601 (2019).
30. Perczel, J. et al. Photonic band structure of two-dimensional atomic lattices. *Phys. Rev. A* **96**, 063801 (2017).
31. Wang, B. X. & Zhao, C. Y. Topological photonic states in one-dimensional dimerized ultracold atomic chains. *Phys. Rev. A* **98**, 023808 (2018).
32. Perczel, J. et al. Topological quantum optics using atom-like emitter arrays coupled to photonic crystals. Preprint at <https://arxiv.org/abs/1810.12299> (2018).
33. Yuan, L., Lin, Q., Xiao, M. & Fan, S. Synthetic dimension in photonics. *Optica* **5**, 1396 (2018).
34. Ozawa, T. & Price, H. M. Topological quantum matter in synthetic dimensions. *Nat. Rev. Phys.* **1**, 349 (2019).
35. Lohse, M. et al. Exploring 4D quantum Hall physics with a 2D topological charge pump. *Nature* **553**, 55 (2018).
36. Zilberberg, O. et al. Photonic topological boundary pumping as a probe of 4D quantum Hall physics. *Nature* **553**, 59 (2018).
37. Lustig, E. et al. Photonic topological insulator in synthetic dimensions. *Nature* **567**, 356 (2019).
38. Dutt, A. et al. Experimental band structure spectroscopy along a synthetic dimension. *Nat. Commun.* **10**, 3122 (2019).
39. Lang, L., Cai, X. & Chen, S. Edge states and topological phases in one-dimensional optical superlattices. *Phys. Rev. Lett.* **108**, 220401 (2012).
40. Kraus, Y. E. et al. Topological states and adiabatic pumping in quasicrystals. *Phys. Rev. Lett.* **109**, 106402 (2012).
41. Poshakinskiy, A. V., Poddubny, A. N., Pillozzi, L. & Ivchenko, E. L. Radiative topological states in resonant photonic crystals. *Phys. Rev. Lett.* **112**, 107403 (2014).
42. Morice, O., Castin, Y. & Dalibard, J. Refractive index of a dilute Bose gas. *Phys. Rev. A* **51**, 3896 (1995).
43. Shang, C., Chen, X., Luo, W. & Ye, F. Quantum anomalous Hall-quantum spin Hall effect in optical superlattices. *Opt. Lett.* **43**, 275 (2018).
44. Hofstadter, D. R. Energy levels and wave functions of Bloch electrons in rational and irrational magnetic fields. *Phys. Rev. B* **14**, 2239 (1976).
45. Olmos, B. et al. Long-range interacting many-body systems with alkaline-earth-metal atoms. *Phys. Rev. Lett.* **110**, 143602 (2013).
46. Syzranov, S. V., Wall, M. L., Gurarie, V. & Rey, A. M. Emergent Weyl excitations in systems of polar particles. *Nat. Commun.* **7**, 13543 (2016).
47. Tokura, Y., van der Wiel, W. G., Obata, T. & Tarucha, S. *Phys. Rev. Lett.* **96**, 047202 (2006).
48. Pioro-Ladrière, M. et al. Electrically driven single-electron spin resonance in a slanting Zeeman field. *Nat. Phys.* **4**, 776 (2008).
49. West, A. D. et al. Realization of the manipulation of ultracold atoms with a reconfigurable nanomagnetic system of domain walls. *Nano Lett.* **12**, 4065 (2012).
50. Anderson, B. M., Spielman, I. B. & Juzeliūnas, G. Magnetically generated spin-orbit coupling for ultracold atoms. *Phys. Rev. Lett.* **111**, 125301 (2013).
51. Luo, X. et al. Generating an effective magnetic lattice for ultracold atoms. *N. J. Phys.* **17**, 083048 (2015).
52. Wang, Y. et al. Magnetic lattices for ultracold atoms and degenerate quantum gases. *Sci. Bull.* **61**, 1097 (2016).
53. Yu, J., Xu, Z., Lü, R. & You, L. Dynamical generation of topological magnetic lattices for ultracold atoms. *Phys. Rev. Lett.* **116**, 143003 (2016).
54. Kitching, J., Knappe, S. & Donley, E. A. Atomic sensors—a review. *IEEE Sens. J.* **11**, 1749 (2011).
55. Roof, S. J., Kemp, K. J., Havey, M. D. & Sokolov, I. M. Observation of single-photon superradiance and the cooperative lamb shift in an extended sample of cold atoms. *Phys. Rev. Lett.* **117**, 073003 (2016).
56. von Diezmann, A., Shechtman, Y. & Moerner, W. E. Three-dimensional localization of single molecules for super-resolution imaging and single-particle tracking. *Chem. Rev.* **117**, 7244 (2017).

Acknowledgements

This paper is supported by the National Natural Science Foundation of China (11734011 and 11974245), the National Key R&D Program of China (2017YFA0303701), and the Natural Science Foundation of Shanghai (19ZR1475700). V.V.Y. acknowledges partial support of the National Science Foundation (NSF) (ECCS-1509268, CMMI-1826078) and Air Force Office of Scientific Research (FA9550-18-1-0141).

Author contributions

A.Z. and L.W. contributed equally to this work. L.Y. initiated the idea. A.Z., L.W., and L.Y. developed the theory, conducted calculations, and performed simulations. X.C., V.V.Y., and L.Y. discussed the results. All authors contributed to writing the paper. L.Y. supervised the project.

Competing interests

The authors declare no competing interests.

Additional information

Supplementary information is available for this paper at <https://doi.org/10.1038/s42005-019-0263-0>.

Correspondence and requests for materials should be addressed to L.Y.

Reprints and permission information is available at <http://www.nature.com/reprints>

Publisher's note Springer Nature remains neutral with regard to jurisdictional claims in published maps and institutional affiliations.



Open Access This article is licensed under a Creative Commons Attribution 4.0 International License, which permits use, sharing, adaptation, distribution and reproduction in any medium or format, as long as you give appropriate credit to the original author(s) and the source, provide a link to the Creative Commons license, and indicate if changes were made. The images or other third party material in this article are included in the article's Creative Commons license, unless indicated otherwise in a credit line to the material. If material is not included in the article's Creative Commons license and your intended use is not permitted by statutory regulation or exceeds the permitted use, you will need to obtain permission directly from the copyright holder. To view a copy of this license, visit <http://creativecommons.org/licenses/by/4.0/>.

© The Author(s) 2019